

DETC2015/47515

REFINED THEORETICAL MODELING OF A NEW-GENERATION PRESSURE-OPERATED SOFT SNAKE

Ming Luo, Yixiao Pan, Weijia Tao, Fuchen Chen, Erik H. Skorina, Cagdas D.Onal*

Mechanical Engineering Department, Robotics Engineering Program

Worcester Polytechnic Institute

Worcester, MA, 01609

Email:{mluo,ypan2, fchen, wtao, ehskorina, cdonal}@wpi.edu

ABSTRACT

Our pressure-operated soft snake robot promises inherent flexibility and versatility to operate on complex and unpredictable environments compared to traditional snake robots made of rigid linkage chains. We previously presented a theoretical framework to describe its unique dynamic behavior and experimentally verified the accuracy of this model. This previous work had some drawbacks; the maximum center of mass velocity of the previous soft snake was one tenth its body length per second and the dynamic model could not predict the behavior of the robot when following non-linear trajectories because of a lack of frictional torques. In this paper we introduce the next generation of our soft robotic snake we call the “WPI SRS”, which can locomote ten times faster than the previous version. Additionally, we present refinements to the dynamical model that can predict both linear and rotational motions of the robot. Finally, we demonstrate the accuracy of this refined model through experimentation.

1 INTRODUCTION

Snake robots [1–3] offer many advantages over other types of mobile robots. Inspired by its biological counterpart, a snake robot could traverse unstructured terrain while being able to pass through narrow openings or complex passages. However, the existing snake robots are made with rigid links, so their fundamental rigidity makes them unable to achieve the same flexibility as

a real snake. To address this issue, we have been developing and testing a series of pneumatically-operated soft robotic snakes to enable the full range of possibilities snake-like undulatory locomotion offers. In addition to the design and fabrication of these robotic snakes, we have also been developing a dynamic model, controller, and planner that would allow them to perform the desired actions.

To this end we previously presented a novel pressure-operated soft robotic snake [4]. The body of this soft robotic snake prototype comprised four bidirectional fluidic elastomer actuators (FEAs) composed in series as actuator-segments pressurized by controlling the state of a solenoid valve array. Similar to other soft robots [5–10], our soft snake robot is inherently safe and adaptable under unpredictable environments, which promises to reduce the burden on planning and control algorithms.

Our previous work also presented a theoretical dynamic model of the soft snake robot and experimentally verified its accuracy over linear motion trajectories [4]. This approach treated each soft segment as an actuated bending joint with solid connectors between segments as links. This model combined a kinematic model, inspired by rigid snake modeling efforts [11–13] with a dynamic model for pneumatic soft actuators [14].

However, there are some parts of the previous work that should be improved. First, the original prototype of the soft snake was slow, with a maximum velocity of its center of mass (CoM) only around 20 mm/s, which is only one tenth its whole body length. This resulted from the inability of the soft actuators

*Address all correspondence to cdonal@wpi.edu.

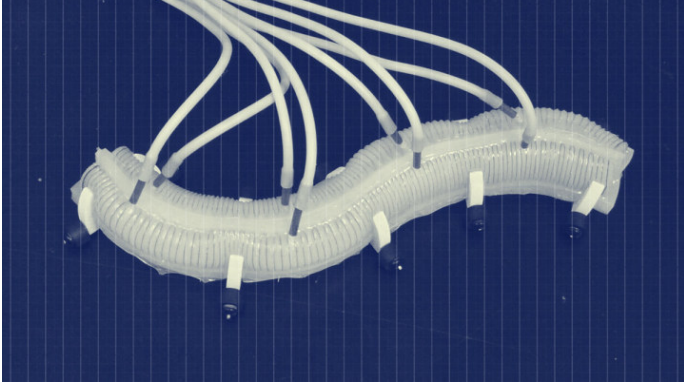


FIGURE 1. Experimental prototype of our new-generation pressure-operated soft robotic snake (WPI SRS), comprising four bidirectional bending soft segments in series and passive wheels at the ends of each segment to generate the necessary frictional anisotropy for lateral undulation.

to tolerate pressures higher than 35 kPa, as well as their loss of energy in the radial direction when pressurized [15]. In addition, the response times of the actuators were long because of the large pneumatic impedance caused by their use of small air channels. Finally, the previous model could not predict the rotational motion of the snake, because it didn't take into account the moments caused by frictional forces.

In this paper, we introduce a new version of the soft robotic snake shown in Figure 1 (called the Worcester Polytechnic Institute Soft Robotic Snake, or "WPI SRS") which uses a more efficient and higher performance bending actuator [15] called the Reverse Pneumatic Artificial Muscle. In addition, we propose a pair of refined snake dynamic models, which include the frictional torque effects. We compare these refined models with experimental results to evaluate their accuracy in predicting linear and rotational motions of the SRS and identify sources of error.

The contributions of this work include:

1. The introduction of a higher performance soft robotic snake with improved linear velocities.
2. The introduction of two dynamic models, which can predict both the linear and the rotational motions of the SRS.

2 REFINED DYNAMIC MODEL

2.1 COMPLEX MODEL

As in our prior analytical model, we examine the balance of forces and torques for each end of each segment (Figure 2). Table 1 lists all the kinematic and dynamic parameters of the SRS model. However, compared with the previous model, the refined model incorporates the moment arms of the soft segments, which are graphically depicted in Figure 3. From this, the force balance

TABLE 1. Parameters of the SRS Dynamic Model

Symbol	Description
N	Number of links
l	The channel length of the soft segment
m	Mass of each link
J	Moment of inertia of each link
μ_t	Tangential coefficient of friction of each link
μ_n	Normal coefficient of friction of each link
$\theta \in \mathbb{R}^N$	Link global orientation vector
$\kappa \in \mathbb{R}^{N-1}$	Segment curvature vector
$\mathbf{X}, \mathbf{Y} \in \mathbb{R}^N$	Link CoM global coordinates vectors
(p_x, p_y)	Global coordinates of the CoM of the robot
$\mathbf{T} \in \mathbb{R}^{N-1}$	Segment torque input vector
$\mathbf{f}_{R,x}, \mathbf{f}_{R,y} \in \mathbb{R}^N$	Ground friction force vectors
$\mathbf{h}_x, \mathbf{h}_y \in \mathbb{R}^{N-1}$	Joint constraint force vectors

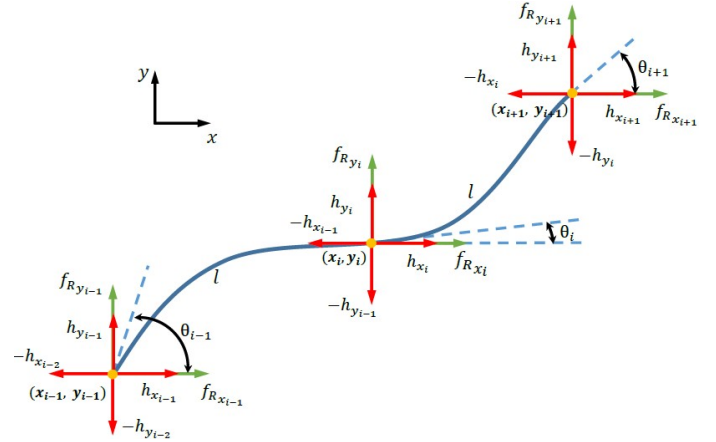


FIGURE 2. The refined complex model of a soft robotic snake.

equation can be written as:

$$\begin{aligned} m\ddot{\mathbf{X}} &= \mathbf{f}_{R,x} + \mathbf{D}^T \mathbf{h}_x, \\ m\ddot{\mathbf{Y}} &= \mathbf{f}_{R,y} + \mathbf{D}^T \mathbf{h}_y. \end{aligned} \quad (1)$$

Figure 3 displays the torque balance for each soft segment. F_{Li} and F_{Ri} represent the external forces perpendicular to the moment arm for points A and B on segment i , which include the joint constraint force and friction. Joint constraint forces ensure that two segments remain connected and frictional forces are

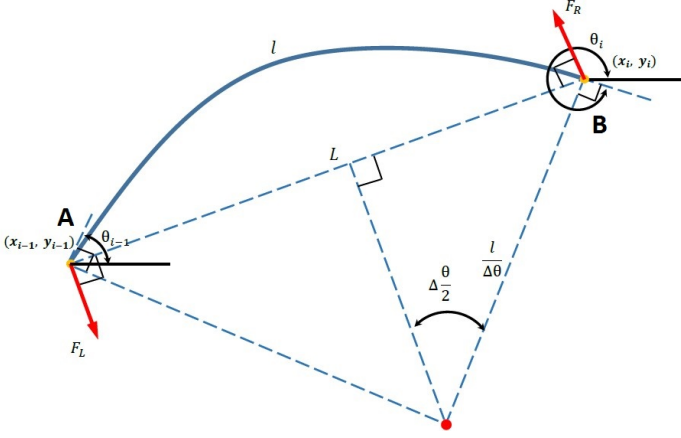


FIGURE 3. The moment arm of each segment of the SRS varies as a function of bending curvature.

anisotropic between the tangential and normal directions [14]. In order to calculate these moment generating forces, the sum of the joint constraint force and friction in Figure 2 should be projected to the moment arm normal direction. The projection angles $\theta_{F_{Li}}$, $\theta_{F_{Ri}}$, respectively for A and B can be calculated by:

$$\text{For point A: } \theta_{F_{Li}} = \frac{\pi}{2} + \frac{\theta_{i-1}}{2} + \frac{\theta_i}{2}$$

$$\text{For point B: } \theta_{F_{Ri}} = \frac{3\pi}{2} + \frac{\theta_i}{2} + \frac{\theta_{i+1}}{2}$$

Let $h_{x,i}^*$, $f_{R_{x,i}}^*$ be the constraint and friction forces in line with the moment generating force on segment i , written as:

$$\begin{aligned} h_{x,i}^* &= h_{x,i} \cos(\theta_{Ri}) + h_{y,i} \sin(\theta_{Ri}) \\ f_{R_{x,i}}^* &= f_{R_{x,i}} \cos(\theta_{Ri}) + f_{R_{y,i}} \sin(\theta_{Ri}) \end{aligned} \quad (2)$$

The length of the moment arm changes as the segment curvature changes. According to the geometric relation shown in Figure 3, the length of the moment arm is given by:

$$l_i = 2 \left| \frac{l}{\Delta\theta} \sin \frac{\Delta\theta}{2} \right| \quad (3)$$

The approximated inertia of each soft actuator end point is given by:

$$j(i) = \begin{cases} 1/3ml_1^2 & \text{if } i = 1 \\ 1/3ml_{N-1}^2 & \text{if } i = N \\ 1/3(ml_{i-1}^2 + ml_i^2) & \text{otherwise} \end{cases}$$

The moment of inertia matrix of the entire soft snake is, then:

$$\mathbf{J} = \begin{pmatrix} j(1) & 0 & & \\ 0 & j(2) & & \\ & & \ddots & 0 \\ & & & 0 & j(N) \end{pmatrix} \in \mathbb{R}^{N \times N} \quad (4)$$

Therefore, the torque balance equation for segment i is:

$$\begin{aligned} j(i) \ddot{\theta}_i &= T_i - T_{i-1} + l_{i-1}(h_{x,i-1}^* - h_{x,i-2}^*) + l_i(h_{x,i+1}^* - h_{x,i}^*) \\ &\quad + l_{i-1}f_{R_{x,i-1}}^* + l_i f_{R_{x,i+1}}^*, \end{aligned} \quad (5)$$

where T_i is the torque with respect to the i^{th} point generated by the input pressure and material deformation [8]. Defining $t_i = \frac{\theta_{i-1}}{2} + \frac{\theta_i}{2}$, we can plug equations (3) and (4) into (5) to reveal the torque balance for the entire snake:

$$\begin{aligned} \mathbf{J} \ddot{\boldsymbol{\theta}} &= \mathbf{D}^T \mathbf{T} - \mathbf{H}_1 \mathbf{C}_1 \mathbf{h}_x + \mathbf{H}_2 \mathbf{C}_1 \mathbf{h}_x + \mathbf{H}_3 \mathbf{C}_2 \mathbf{h}_y - \mathbf{H}_4 \mathbf{C}_2 \mathbf{h}_y \\ &\quad - \mathbf{H}_5 \mathbf{f}_{R,x} + \mathbf{H}_7 \mathbf{f}_{R,x} + \mathbf{H}_6 \mathbf{f}_{R,y} - \mathbf{H}_8 \mathbf{f}_{R,y} \end{aligned} \quad (6)$$

$$\begin{aligned} \mathbf{H}_1 &= \mathbf{A}_1 \text{ where } C_{i,i} = l_{i-1} \sin t_{i-1} \\ \mathbf{H}_2 &= \mathbf{A}_1 \text{ where } C_{i,i} = l_{i-1} \cos t_{i-1} \\ \mathbf{H}_3 &= \mathbf{A}_2 \text{ where } C_{i,i} = l_i \sin t_i \\ \mathbf{H}_4 &= \mathbf{A}_2 \text{ where } C_{i,i} = l_i \cos t_i \\ \mathbf{H}_5 &= \mathbf{A}_3 \text{ where } C_{i,i-1} = l_{i-1} \sin t_{i-1} \\ \mathbf{H}_6 &= \mathbf{A}_4 \text{ where } C_{i,i-1} = l_{i-1} \cos t_{i-1} \\ \mathbf{H}_7 &= \mathbf{A}_3 \text{ where } C_{i,i+1} = l_i \sin t_i \\ \mathbf{H}_8 &= \mathbf{A}_4 \text{ where } C_{i,i+1} = l_i \cos t_i \end{aligned}$$

Equations (7) describe below the format of the matrices H_1 through H_8 for the given C elements for each case:

$$\begin{aligned} \mathbf{A}_1 &= \begin{pmatrix} 0 & 0 \\ 0 & C_{2,2} \\ & \ddots & \ddots \\ & 0 & C_{N-1,N-1} \\ & & & 0 & C_{N,N} \end{pmatrix}, \mathbf{A}_2 = \begin{pmatrix} C_{1,1} & 0 \\ 0 & C_{2,2} \\ & \ddots & \ddots \\ & & C_{N-1,N-1} & 0 \\ & & & 0 & 0 \end{pmatrix} \in \mathbb{R}^{N \times N} \\ \mathbf{A}_3 &= \begin{pmatrix} 0 & 0 \\ C_{2,1} & 0 \\ & \ddots & \ddots \\ & 0 & 0 \\ & & C_{N,N-1} & 0 \end{pmatrix}, \mathbf{A}_4 = \begin{pmatrix} 0 & C_{1,1} \\ 0 & 0 \\ & \ddots & \ddots \\ & 0 & C_{N-1,N-1} \\ & & 0 & 0 \end{pmatrix} \in \mathbb{R}^{N \times N} \\ \mathbf{C}_1 &= \begin{pmatrix} 0 & 0 \\ 1 & 0 \\ & \ddots & \ddots \\ & 1 & 0 \\ & & -1 & 1 \end{pmatrix}, \mathbf{C}_2 = \begin{pmatrix} -1 & 1 \\ 0 & -1 \\ & \ddots & \ddots \\ & 0 & -1 \\ & & 0 & 0 \end{pmatrix} \in \mathbb{R}^{N \times (N-1)} \end{aligned} \quad (7)$$

We can combine Equations (1) and (6) to yield:

$$\begin{aligned} \mathbf{M}_\theta \ddot{\boldsymbol{\theta}} + \mathbf{W}_\theta \dot{\boldsymbol{\theta}}^2 + \mathbf{G}_\theta \dot{\boldsymbol{\theta}} + \mathbf{M}_\kappa \ddot{\boldsymbol{\kappa}} + \mathbf{W}_\kappa \dot{\boldsymbol{\kappa}}^2 + \mathbf{F}_1 \mathbf{f}_{R,x} + \mathbf{F}_2 \mathbf{f}_{R,y} &= \mathbf{D}^T \mathbf{T} \\ Nm[\ddot{\mathbf{X}}\dot{\mathbf{Y}}]^T &= \mathbf{E}^T \mathbf{f}_R \end{aligned} \quad (8)$$

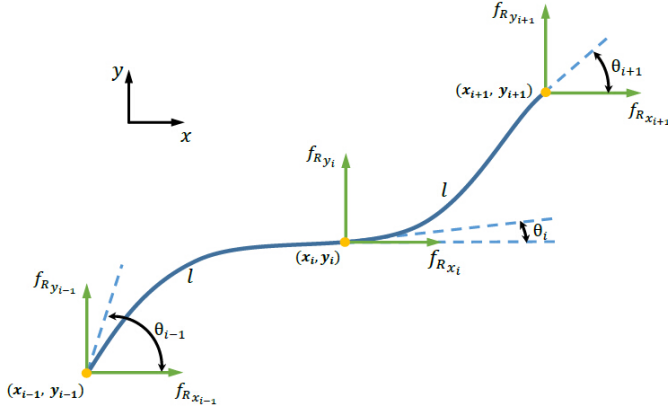


FIGURE 4. The refined simplified model of a soft robotic snake.

$$\begin{aligned}
M_\theta &= JI_N + mlH_9(DD^T)^{-1}B_1 + mlH_{10}(DD^T)^{-1}B_3 \\
W_\theta &= mlH_9(DD^T)^{-1}B_3 - mlH_{10}(DD^T)^{-1}B_1 \\
G_\theta &= mlH_9(DD^T)^{-1}B_4 + mlH_{10}(DD^T)^{-1}B_7 \\
M_\kappa &= mlH_9(DD^T)^{-1}B_5 + mlH_{10}(DD^T)^{-1}B_8 \\
W_\kappa &= mlH_9(DD^T)^{-1}B_6 + mlH_{10}(DD^T)^{-1}B_9 \\
F_1 &= H_{11}(DD^T)^{-1}D - H_{13} \\
F_2 &= -H_{12}(DD^T)^{-1}D + H_{14} \\
E &= \begin{pmatrix} \mathbf{e} & \mathbf{0}_{N \times 1} \\ \mathbf{0}_{N \times 1} & \mathbf{e} \end{pmatrix} \in \mathbb{R}^{2N \times 2} \\
\mathbf{e} &= (1, \dots, 1)^T \in \mathbb{R}^N
\end{aligned} \tag{9}$$

$$H_9 = (H_3C_2 - H_1C_1), H_{10} = (H_4C_2 - H_2C_1), H_{11} = (H_3 - H_1), H_{12} = (H_4 - H_2), H_{13} = (H_7 - H_5), H_{14} = (H_8 - H_6).$$

This set of equations provides an accurate mathematical representation of the ideal dynamics of our soft snake robot. However, as the same as previous dynamic modeling [4], the complete model is computationally expensive because of the joint constraint force calculations. In the next section, we present a simplified model, which ignores joint constraint forces.

2.2 SIMPLIFIED MODEL

Figure 4 displays a diagram of the simplified dynamics modeling. Without the joint constraint force, the force balance equation can be rewritten as:

$$\begin{aligned}
m\ddot{\mathbf{X}} &= \mathbf{f}_{R,x}, \\
m\ddot{\mathbf{Y}} &= \mathbf{f}_{R,y},
\end{aligned} \tag{10}$$

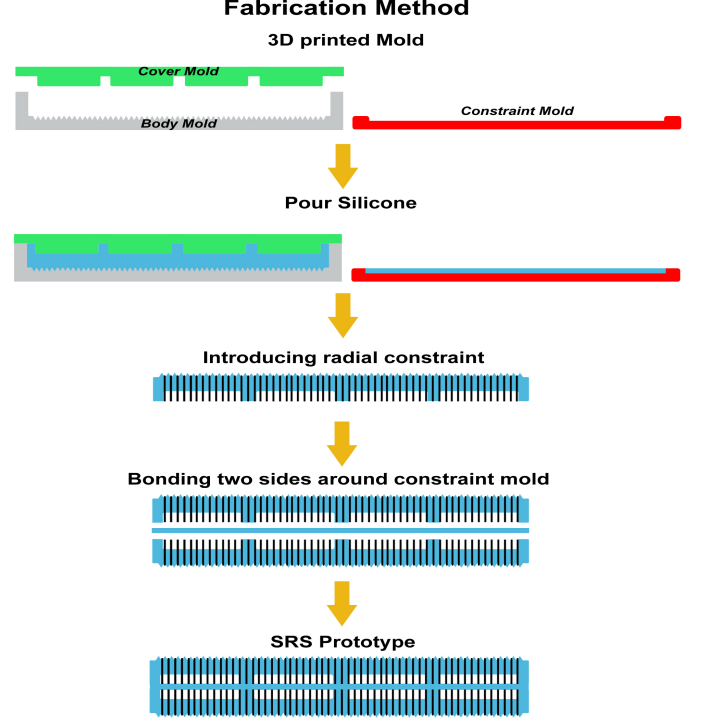


FIGURE 5. Fabrication process of the proposed soft robotic snake.

and the torque balance equation for all links is rewritten as:

$$J\ddot{\theta} = D^T T - H_5 \mathbf{f}_{R,x} + H_7 \mathbf{f}_{R,x} + H_6 \mathbf{f}_{R,y} - H_8 \mathbf{f}_{R,y} \tag{11}$$

Combining Equations (10) and (11), the dynamics of the whole system can be rewritten as:

$$\begin{aligned}
M_\theta \ddot{\theta} - H_{13} \mathbf{f}_{R,x} + H_{14} \mathbf{f}_{R,y} &= D^T T \\
Nm[\ddot{\mathbf{X}}\ddot{\mathbf{Y}}]^T &= E^T \mathbf{f}_R,
\end{aligned} \tag{12}$$

where $M_\theta = JI_N$.

3 EXPERIMENTAL SETUP

3.1 FABRICATION

Compared with the original fluidic elastomer actuators (FEA) [16], we recently introduced an actuator, which offers robust operation, safety at larger input pressure values, faster response, lower center of gravity, and a flat bottom for better compatibility with snake-like lateral undulation in prior work [15]. The entire fabrication process of the SRS, which uses four bidirectional bending actuators as segments, consists of four steps as explained below and illustrated in Figure 5:

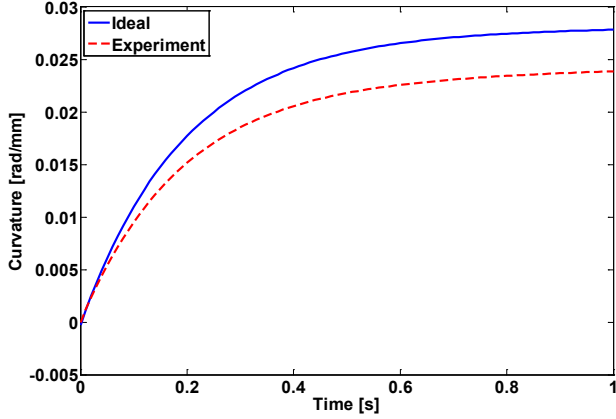


FIGURE 6. Dynamic response of the fludic elastomer actuators under 62 kPa. The blue line represent the ideal case without frictional forces and the red line represents the experimental case.

Step 1 Body mold and constraint mold are 3D printed. The body mold has two parts, the holder which has the main shape of the actuator and the cover which helps form the shape of the channel. Constraint mold is a rectangular shell. An inextensible flexible sheet is inserted into the constraint mold.

Step 2 The silicone is poured into all molds. After the silicone fills the body mold, the cover is placed on top to create the fluidic channel. The silicone cures at room temperature in four hours. Two half bodies and the constraint layer are made at the same time.

Step 3 Half bodies are demolded. Nylon thread is tied following circular grooves around the body. A small amount of uncured silicone is brushed to cover the thread to make sure it stays in place attached to the main body.

Step 4 Finally, two half bodies and constraint layer are bonded to each other using a very thin layer of uncured silicone.

3.2 CONTROL

The WPI SRS uses a lateral undulation gait for locomotion. In the SRS, control inputs are the states of the solenoid valves. Each segment is controlled by two parallel solenoid valves operating antagonistically, each controlling a single bending direction. In order to generate a traveling curvature wave, the operation states of the solenoid valves are controlled by:

$$S_i = \text{sign}(\sin(\omega t + \beta_i) + \phi), \quad (13)$$

where ω , β_i and ϕ are the frequency, traveling wave delay, and offset of the i^{th} actuator, respectively. The solenoid valve is open when $S_i > 0$ and is closed otherwise.

Since the SRS is an underactuated system [4], (8) and (12) were rewritten in state vector form, where a feedback linearized

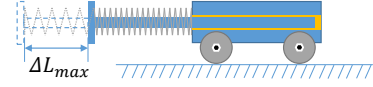


FIGURE 7. The friction measurement platform comprises the same passive wheels used in the SRS at the ends of each segment and a force measurement system, such that coefficients of friction can be characterized.

TABLE 2. EXPERIMENTAL PARAMETERS

N	l	m	μ_t	μ_n	β_i
5	0.037 m	0.03 kg	0.043	0.57	$\frac{2\pi i}{N-1}$

formulation enables direct control of each segment's curvature, while the global angle of the tail and the CoM velocities are indirectly controlled through segment curvatures.

Based on experimental characterizations, the dynamic response of the actuator behaves as a second-order system [14]:

$$\kappa = C_1 e^{(-t/\tau_1)} + C_2 e^{(-t/\tau_2)} + C_0, \quad (14)$$

where τ_1, τ_2 are time constants and C_0, C_1 , and C_2 are constant parameters. Combining Equations (13) and (14), segment curvature dynamics are written as:

$$\ddot{\kappa} = -\left(\frac{1}{\tau_1} + \frac{1}{\tau_2}\right)\dot{\kappa} - \left(\frac{1}{\tau_1\tau_2}\right)\kappa + \frac{C_0}{\tau_1\tau_2}S_i \quad (15)$$

3.3 MOTION TRACKING

In order to verify our dynamic model, we built an overhead motion tracking system for our snake robot. To ensure stability in the tracking procedure, we used an Optitrack V120:SLIM camera and infrared (IR) LEDs as tracking markers. In order to track the whole body movement, we mounted these IR markers on top of each snake segment and calculated the curvature variation for each segment based on the marker position data.

4 RESULTS

4.1 FRICTIONAL CHARACTERIZATION

In order to ensure the model's accuracy, the friction between the contact surface and the snake's passive wheels needs to be considered in the dynamic actuator modeling. Figure 6 shows the two cases of the dynamic response behavior of the actuator with and without friction. The addition of friction forces reduces the amplitude C_0 and increase the time constants τ_1, τ_2 in (14) under experimental conditions.

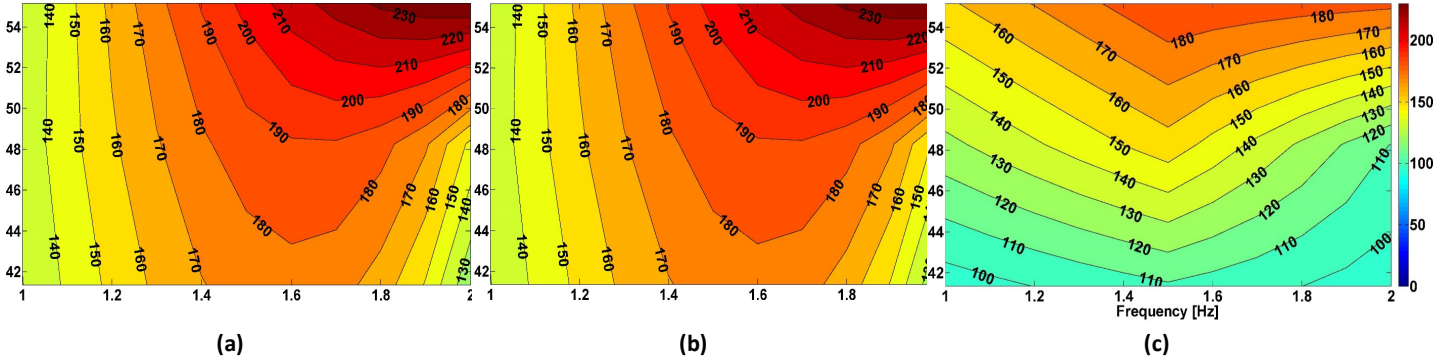


FIGURE 8. Comparison of model predictions and experimental results for different operational parameters of the soft robotic snake in terms of resulting CoM velocities with the offset term $\phi = 0$. The frequencies from 1 to 2 Hz (x-axis) and pressure inputs ranging from 41 to 55 kpa (y-axis). (a),(b),(c) are the CoM velocities for complex model simulation, simplified model simulation and experimental results when $\phi = 0$.

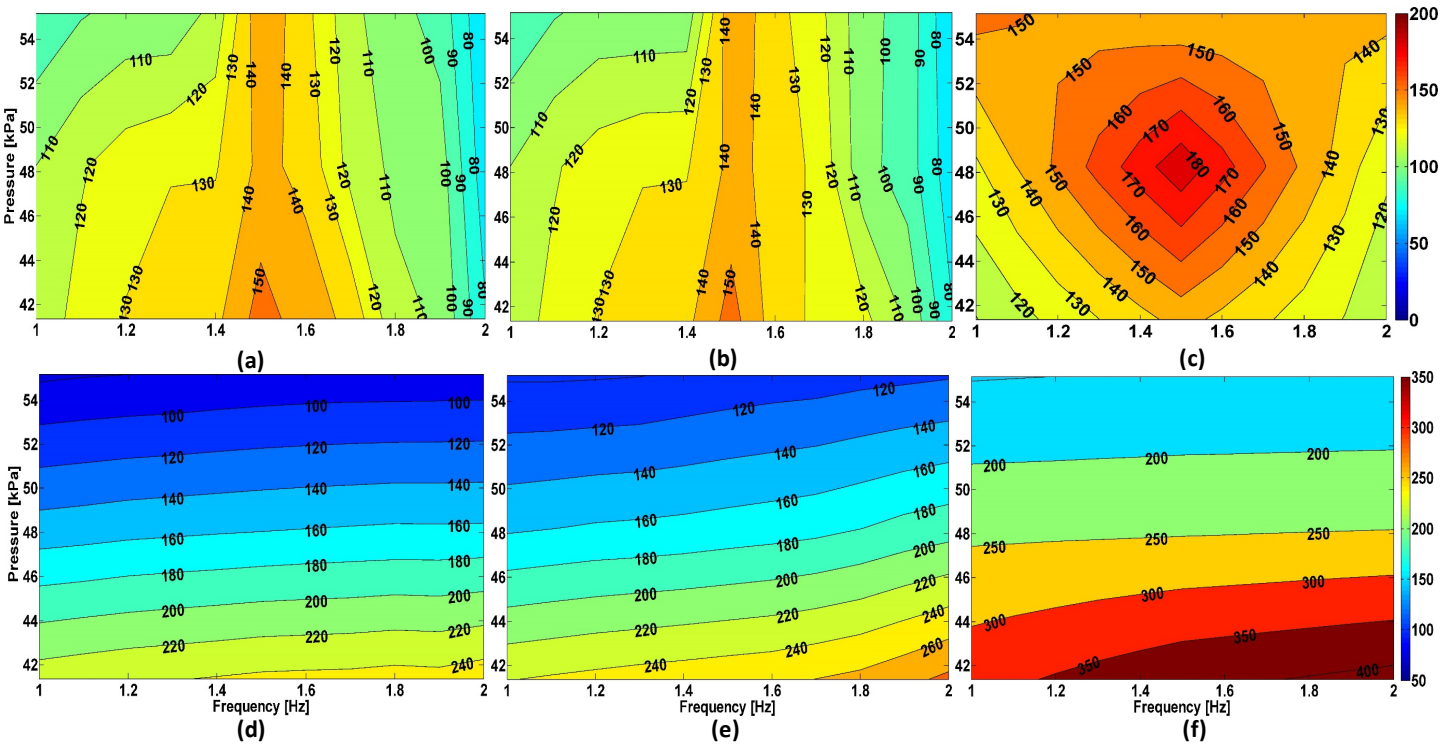


FIGURE 9. Comparison of model predictions and experimental results for different operational parameters of the soft robotic snake in terms of resulting CoM velocities and trajectory radii with the offset term $\phi = 0.4$. The frequencies from 1 to 2 Hz (x-axis) and pressure inputs ranging from 41 to 55 kpa (y-axis). (a),(b),(c) are the CoM velocities for complex model simulation, simplified model simulation and experimental results when $\phi = 0.4$. (d),(e),(f) show the complex model simulation, simplified model simulation, and experimental turning radius of the CoM when $\phi = 0.4$.

Coulomb friction coefficients are key to the dynamic behavior of the snake robot. To obtain accurate friction coefficients, we utilized a “spring car” shown in Figure 7, which included a spring of known stiffness, a linear potentiometer, and passive wheels. As the contact forces are gradually increased, the car starts moving. To simulate friction forces in both tangential and

normal directions with respect to the snake body, we recorded the largest deformation of the spring ΔL_{max} , when wheels are freely rotating and when they are fixed. The friction coefficients were

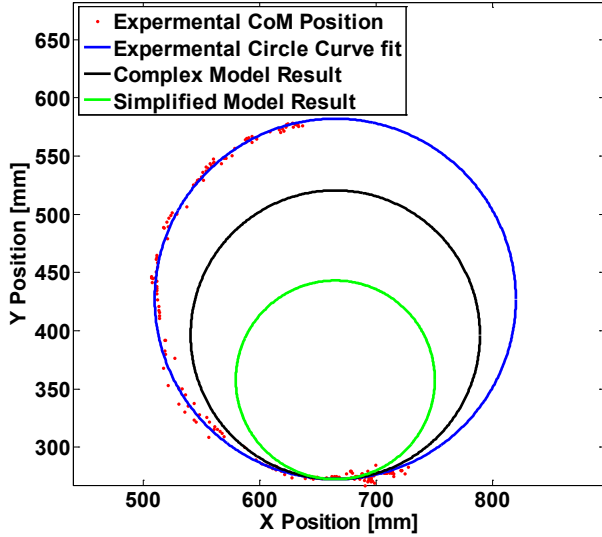


FIGURE 10. A plot of the experimental trajectory (red dots) and fit line (blue line) compared to the complex and simple model trajectories (black and green lines) with frequency 2 Hz and input pressure 54 kPa.

simply calculated as:

$$\mu = \frac{k\Delta L_{max}}{mg}. \quad (16)$$

The measured parameters are listed in Table 2.

4.2 COMPUTATIONAL COST OF BOTH MODELS

To compare the computational cost (measured as total runtime) of the two models in a simulation environment, we used the Matlab ODE toolbox to solve the differential equations of the soft snake robot model. The inputs to the simulation were the dynamic parameters of each actuator under friction as shown in Equation (15) and a traveling waveform of solenoid valve on/off commands calculated from (13) for a total of 500 seconds of undulatory locomotion. Simulations ran on a desktop computer with an Intel Core i7 2.80 GHz CPU and Windows 7 operating system. The complex model was solved in 94 seconds, while the simplified model was solved in 69 seconds, a 27% improvement.

4.3 EXPERIMENTAL VERIFICATION

To evaluate the strength of the refined model in describing the dynamic behavior of our soft robotic snake, we compared the model performance to that of the physical SRS. Figure 8 displays contour plots of CoM velocities for the simulated model predictions and experimental results when offset $\phi = 0$. Input pressures ranged from 41 to 55 kPa and the frequency ranged from 1 to 2 Hz. SRS travels in a straight line when $\phi = 0$. The

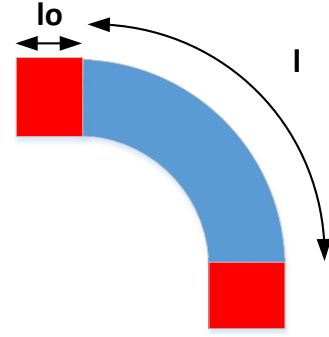


FIGURE 11. A diagram of each segment. The actuator with an interior pressure chamber is the blue area, while the red areas are the gaps. Only blue area is pressurized and capable of active motion.

maximum linear velocity is around 220 mm/s which is ten times faster than the previous snake robot. The results shows that both model predictions are similar to the experimental results with the complex model being slightly closer.

Figure 9(a-c) shows the contour plots of CoM velocities for the simulated model predictions and experimental results when offset $\phi = 0.4$. While the general behavior is captured by both models, the simplified model seems to predict the CoM velocity better for the offset value. The differences that exist between the two predictions and experimental results are likely caused by several factors, including measurement error, fabrication inconsistencies, and the forces due to external tubing, especially for rotation motion. The snake was driven by an external air pressure source and the weight and friction of the required tubing was likely a factor in skewing the results of this experiment. In addition, the fabrication inconsistencies caused the constraint layer between the two halves of the body to have a non-trivial and varying width, changing the behavior of the snake.

Figure 9(d-f) shows the contour plots of the turning radius for the same simulated model predictions and experimental results when offset $\phi = 0.4$. Similarly, a strong dependence of turning radii values on input pressure is revealed for all cases, but predictions are off by wide margin. Figure 10 shows the center of mass trajectory from the motion capture system and its corresponding circle fit alongside the predicted trajectories with frequency 2 Hz and input pressure 54 kPa. In the simulation, the length l of each segment was also assumed to be the length of the pressure chamber assuming the gap between the channels are negligible. However, these unactuated portions do not provide torque and impede the actuator bending, which reduces the SRS' ability to turn (see Figure 11). Therefore, we choose a correction factor $((l + L_o)/l)$ that represents the ratio of the total segment length including the gap, divided by the length of the channel. We multiplied this factor with the measured radius values (or rotational velocities) in the simulation results. The experimental

turning radius values are still larger than the predictions of the two models, with the complex model results being closer. One of the reasons for this mismatch, in addition to experimental errors mentioned above, is that the models do not include the passive bending forces occurring at these portions, which act to reduce actuator bending curvatures and increase turning radii. Nevertheless, these investigations indicate that, through an initial calibration routine, the proposed models are strong enough to predict the CoM motions of the SRS following non-linear trajectories as a level of abstraction to a non-holonomic differential drive mobile robot, which in turn, makes planning and higher-level control tasks easier.

5 Conclusions and Future Work

This article introduced a new generation soft snake robot we call the WPI Soft Robotic Snake or WPI SRS, made of silicone rubber that can achieve velocities ten times faster than the previous generation snake robot. In addition, we refined our dynamic model which allowed it to predict not only the snake's CoM velocity when undergoing straight motion but also its velocity and the turning radius when undergoing rotational motion. In order to control this soft snake motion based on our model for future studies, we need to make the soft snake move freely in a large area. However, the workspace of our current soft snake robot is limited by the external air, power source and tubing.

Future work will focus on a self-contained SRS, which will include electrical and pressure power sources, on-board control and embedded curvature sensors [17], which can measure the bending angle of each actuator. Using the proposed refinement of the soft snake dynamic model, we will be able to use this proposed soft snake robot for more precise control and motion planning. This could include having the snake traverse a maze, where it would need to adjust its undulation parameters in order to move through challenging passages.

REFERENCES

[1] Hirose, S., 1993. *Biologically Inspired Robots: Snake-like Locomotors and Manipulators*. Oxford University Press.

[2] McKenna, J. C., Anhalt, D. J., Bronson, F. M., Brown, H. B., Schwerin, M., Shamma, E., and Choset, H., 2008. "Toroidal skin drive for snake robot locomotion". In *Robotics and Automation, 2008. ICRA 2008. IEEE International Conference on, IEEE*, pp. 1150–1155.

[3] Wright, C., Buchan, A., Brown, B., Geist, J., Schwerin, M., Rollinson, D., Tesch, M., and Choset, H., 2012. "Design and architecture of the unified modular snake robot". In *Robotics and Automation (ICRA), 2012 IEEE International Conference on, IEEE*, pp. 4347–4354.

[4] Luo, M., Agheli, M., and Onal, C. D., 2014. "Theoretical

modeling and experimental analysis of a pressure-operated soft robotic snake". *Soft Robotics*, *1*(2), pp. 136–146.

[5] Trimmer, B. A., Takesian, A. E., Sweet, B. M., Rogers, C. B., Hake, D. C., and Rogers, D. J., 2006. "Caterpillar locomotion: a new model for soft-bodied climbing and burrowing robots". In *7th International Symposium on Technology and the Mine Problem, Vol. 1, Citeseer*, pp. 1–10.

[6] Shepherd, R. F., Ilievski, F., Choi, W., Morin, S. A., Stokes, A. A., Mazzeo, A. D., Chen, X., Wang, M., and Whitesides, G. M., 2011. "Multigait soft robot". *Proceedings of the National Academy of Sciences*, *108*(51), pp. 20400–20403.

[7] Skorina, E. H., Luo, M., Ozel, S., Chen, F., Tao, W., and Onal, C. D., 2015. "Feedforward augmented sliding mode motion control of antagonistic soft pneumatic actuators". In *Robotics and Automation (ICRA), 2015 IEEE International Conference on, IEEE*.

[8] Luo, M., Skorina, E. H., Oo, W. Y., Tao, W., Chen, F., Youssefian, S., Rahbar, N., and Onal, C. D., 2015. "Reverse pneumatic artificial muscles: Modeling, analysis, and integration". *The International Journal of Robotics Research (under review)*.

[9] Luo, M., Skorina, E. H., Tao, W., Chen, F., and Onal, C. D., 2015. "Optimized design of a rigid kinematic module for antagonistic soft actuation". In *Proceedings of the IEEE International Conference on Technologies for Practical Robot Applications*.

[10] Ranzani, T., Cianchetti, M., Gerboni, G., De Falco, I., Petroni, G., and Menciassi, A. "A modular soft manipulator with variable stiffness".

[11] Pettersen, K. Y., Stavdahl, Ø., and Gravedahl, J. T., 2013. *Snake Robots: Modelling, Mechatronics, and Control*. Springer.

[12] Sato, M., Fukaya, M., and Iwasaki, T., 2002. "Serpentine locomotion with robotic snakes". *Control Systems, IEEE*, *22*(1), pp. 64–81.

[13] Ma, S., 2001. "Analysis of creeping locomotion of a snake-like robot". *Advanced Robotics*, *15*(2), pp. 205–224.

[14] Onal, C. D., and D.Rus, 2013. "Autonomous undulatory serpentine locomotion utilizing body dynamics of a fluidic soft robot". *Bioinspiration & biomimetics*, *8*(2), p. 026003.

[15] Luo, M., Tao, W., Chen, F., Khoo, T. K., Ozel, S., and Onal, C. D., 2014. "Design improvements and dynamic characterization on fluidic elastomer actuators for a soft robotic snake". In *Proceedings of the IEEE International Conference on Technologies for Practical Robot Applications*.

[16] Onal, C. D., and Rus, D., 2012. "A modular approach to soft robots". In *Biomedical Robotics and Biomechanics (BioRob), 2012 4th IEEE RAS & EMBS International Conference on, IEEE*, pp. 1038–1045.

[17] Selim Ozel, Nehir A. Keskin, D. K. C. D. O. "Design and verification of an accurate curvature sensor for soft bodied robots". *Sensors and Actuators A: Physical (under Review)*.